Physica E 64 (2014) 95–105

Contents lists available at ScienceDirect

Physica E

journal homepage: www.elsevier.com/locate/physe

Nonlinear free vibrations of curved double walled carbon nanotubes using differential quadrature method

Ender Cigeroglu *, Hamed Samandari

Middle East Technical University, Department of Mechanical Engineering, Ankara 06800, Turkey

HIGHLIGHTS

- Vibrations of curved DWCNTs with geometric & vdW force nonlinearities using DQM are studied.
- Different boundary conditions (BCs) are formulated and studied using DQM.
- Nonlinear mode shape of the CNT cannot be represented by a single linear eigenfunction.
- For symmetric BCs, only the odd modes of the linear system are present in the solution.
- For asymmetrical BCs, both odd and even modes of the linear system are present.

GRAPHICAL ABSTRACT

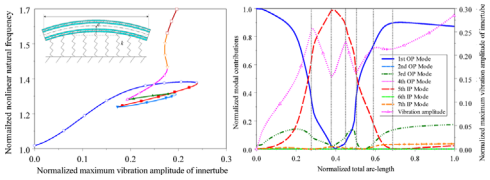

ARTICLE INFO

Article history:
Received 17 May 2014
Received in revised form
28 June 2014
Accepted 9 July 2014
Available online 16 July 2014

Keywords:
Curved carbon nanotubes
Geometric nonlinearity
Van der Waals nonlinearity
Differential quadrature method
Euler–Bernoulli theory

ABSTRACT

Nonlinear free vibration analysis of curved double-walled carbon nanotubes (DWNTs) embedded in an elastic medium is studied in this study. Nonlinearities considered are due to large deflection of carbon nanotubes (geometric nonlinearity) and nonlinear interlayer van der Waals forces between inner and outer tubes. The differential quadrature method (DQM) is utilized to discretize the partial differential equations of motion in spatial domain, which resulted in a nonlinear set of algebraic equations of motion. The effect of nonlinearities, different end conditions, initial curvature, and stiffness of the surrounding elastic medium, and vibrational modes on the nonlinear free vibration of DWCNTs is studied. Results show that it is possible to detect different vibration modes occurring at a single vibration frequency when CNTs vibrate in the out-of-phase vibration mode. Moreover, it is observed that boundary conditions have significant effect on the nonlinear natural frequencies of the DWCNT including multiple solutions.

1. Introduction

After the discovery of carbon nanotubes (CNTs) by Iigima [1], considerable attention has been devoted to carbon nanotubes (CNTs), since they have the ability to revolutionize critical technologies owing to their remarkable physical, mechanical, and electrical properties [2]. These extraordinary properties made CNTs as perfect materials for a wide range of applications [3–5]. CNTs can be efficiently utilized as nano-pipes used in fluid transport and drug delivery systems [6–8]. Also, CNTs have potential applications in nano-actuators, nano-motors, and nano-sensors [9–12].

Recent theoretical and experimental studies show that the deformation of CNTs is nonlinear in nature. Fu et al. [13] investigated the nonlinear free vibration of embedded single and multiple walled CNTs. By using the incremental harmonic balanced

* Corresponding author. Tel.: +90 312 210 2579; fax: +90 312 210 2536.
E-mail address: ender@metu.edu.tr (E. Cigeroglu).

http://dx.doi.org/10.1016/j.physe.2014.07.010
1386-9477/

method, they observed that as vibration amplitude increases, the nonlinear natural frequency increases for uniform simply supported single and double walled CNTs. Later studies show that in the case of multiple walled carbon nanotubes (MWCNTs), natural frequencies of CNTs are affected by another source of nonlinearity, interlayer molecular forces. The interlayer force between layers of CNTs is governed by van der Waals (vdW) force. The vdW force estimated by Lennard-Jones potential is inherently nonlinear [14–16]; therefore, in order to accurately predict the vibrational behavior of MWCNTs, the nonlinear effect of vdW force should be considered [17,18]. The effect of vdW force on nonlinear natural frequencies of DWCNTs is investigated by Cigeroglu and Samandari [19] using describing function method and utilizing multiple trail functions in Galerkin method. It is observed that utilization of multiple trial functions resulted in the determination of multiple nonlinear natural frequencies at the same vibration amplitude and identification of single nonlinear natural frequencies associated with different vibration amplitudes. Even though Galerkin method is easy to implement, it requires trial functions or comparison functions that satisfy all the (geometric and natural) boundary conditions of the system. Hence, Galerkin approach is used only for studying hinged–hinged beams where the trial functions are simple sine functions. Therefore, presenting a general formulation capable of predicting the vibrational behavior of CNTs under different boundary conditions is of high importance. Recently, finite element method (FEM) is proposed to study the free vibration of CNTs where solution method such as Galerkin method is not applicable. Applicability of FEM in studying the free vibration of CNTs is investigated by Ansari et al. [20] in the presence of only geometric nonlinearity. Using FEM, authors were able to study the effect of boundary conditions on nonlinear natural frequencies for the first time. Even though classic FEMs can predict vibrational behavior of CNTs, they are disadvantaged in terms of computational time since they require higher number of grid points which results in large number of nonlinear equations. In order to overcome this difficulty differential quadrature method is utilized in this study.

The differential quadrature method (DQM) is a well-developed numerical method for quick solutions of linear and nonlinear partial differential equations. DQM developed by Bellman and Casti [21] is a discrete approach to directly solve the governing equations of various engineering problems. Different from conventional methods such as finite difference (FD) and finite element (FE) methods, DQM requires less grid points to obtain an acceptable accuracy. A comprehensive review on the DQM can be found in [22]. Owning to its efficiency and accuracy, DQM has the potential to be used in variety of application areas. Applicability of DQM for micro and nanoscale beams and tubes is studied by Civalek et al. [23] and Wang et al. [24] for linear systems. Later, considering the nonlocal effect and temperature effects, same problem has been solved by Zhen and Fang [25]. Based on Eringen's nonlocal elasticity theory and von Kármán geometric nonlinearity, the nonlinear free vibration of a DWCNT is studied by Ke et al. [26] where a direct iterative method is used to solve the resulting system of equations. They studied the effect of system parameters on variation of nonlinear natural frequency of a DWCNT vibrating in the first in-phase vibration mode where different types of boundary conditions are considered. Later, benefiting from the advantages of DQM, Janghorban and Zare [27] studied the linear free vibration of functionally graded carbon nanotubes with variable thickness, where material properties are assumed to be graded in the longitudinal direction and a similar problem using different beam theories is studied by Ansari et al. [28].

The number of nonlinear studies on vibrations of CNTs having different end conditions is rare in literature due to the limitation of Galerkin method explained formerly. In addition to this, it is observed that only geometric nonlinearity is studied in these studies and nonlinear van der Waals effects between the layers of CNTs are neglected, since existence of vdW force complicates the solution. Therefore, to the best of author's knowledge, this is the first study, which considers nonlinear free vibrations of curved double walled carbon nanotubes (DWCNTs) with different types of boundary conditions, where in addition to geometric nonlinearity, nonlinear interlayer van der Waals (vdW) force is also included. Differential quadrature method is used to discretize the partial differential equations of motion resulting in a system of nonlinear ordinary differential equations. The main advantage of DQM, in comparison to solution methods like variational approach [29], or Galerkin method [18,30], is its inherent simplicity in formulation, where different end conditions can be easily adopted. Using DQM and considering a harmonic solution in time, nonlinear differential equations of motion are converted into a set of nonlinear algebraic equations, which is solved by the developed iterative path following method (IPFM).

2. Modeling

Consider a DWCNT of length L, cross-sectional areas A_i, A_o, area moment of inertias I_i, I_o, Young's modules E_i, E_o, and densities ρ_i, ρ_o embedded in an elastic medium having a stiffness per unit length of k as shown in Fig. 1, where i and o indicate the inner and outer tubes, respectively. Assume that the transverse displacements of nanotubes are $w_i(x,t), w_o(x,t)$ where x and t are the spatial coordinate and the temporal variable. Equations of motion for free vibration of embedded curved DWCNTs considering geometric, initial curvature, and vdW force nonlinearities are given as [31–33]

$$E_iI_i\frac{\partial^4 w_i}{\partial x^4}+\rho_iA_i\frac{\partial^2 w_i}{\partial t^2}=\frac{E_iA_i}{L}\int_0^L\left[\frac{dZ}{dx}\frac{\partial w_i}{\partial x}+\frac{1}{2}\left(\frac{\partial w_i}{\partial x}\right)^2\right]dx \times\left(\frac{\partial^2 w_i}{\partial x^2}+\frac{d^2Z}{dx^2}\right)+p_v(x,t), \tag{1}$$

$$E_oI_o\frac{\partial^4 w_o}{\partial x^4}+\rho_oA_o\frac{\partial^2 w_o}{\partial t^2}=\frac{E_oA_o}{L}\int_0^L\left[\frac{dZ}{dx}\frac{\partial w_o}{\partial x}+\frac{1}{2}\left(\frac{\partial w_o}{\partial x}\right)^2\right]dx \times\left(\frac{\partial^2 w_o}{\partial x^2}+\frac{d^2Z}{dx^2}\right)+p_m(x,t)-p_v(x,t) \tag{2}$$

$Z(x)$ is the initial curvature (waviness) of the cylindrical tubes. $p_m(x,t)$ is the contact force between the surrounding medium and the tube which can be identified by Winkler-like model [34,35] and $p_v(x,t)$ is the nonlinear vdW force. According to the Winkler-like model theory, the interaction between surfaces can be simulated as a linear spring resulting in a pressure distribution linearly proportional to the relative displacement between the surfaces as

$$p_m(x,t)=-kw_o(x,t). \tag{3}$$

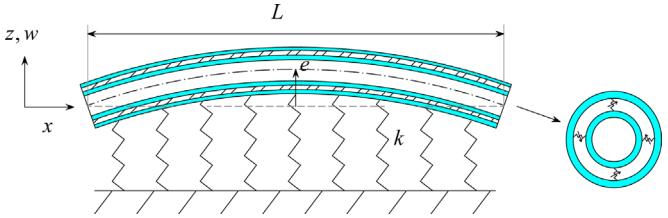

Fig. 1. Model of an embedded curved DWCNT.

The negative sign in the above equation indicates that the pressure is opposite to the deflection of the tube and k is defined by the material constants of the surrounding elastic medium. On the other hand, vdW force is composed of attractive forces between atoms, molecules, and surfaces which only come into action when the relative displacements are comparable with the atom sizes [36,37]. The vdW force per unit area for two originally-concentric tubes is given in [38,39] as

$$p_v(x,t) = p_1(w_o - w_i) + p_2(w_o - w_i)^3, \tag{4}$$

where $p_1 = 2r_i(\partial^2 U/\partial\delta^2)\big|_{\delta=\delta_0}$, $p_2 = 2r_i(1/6)(\partial^4 U/\partial\delta^4)\big|_{\delta=\delta_0}$, r_i is innertube radius, and U is potential energy expressed in terms of the interlayer spacing r_i as follows [18,19]:

$$U(\delta) = K_{IL}\left[\left(\frac{\delta_0}{\delta}\right)^4 - 0.4\left(\frac{\delta_0}{\delta}\right)^{10}\right], \tag{5}$$

where $K_{IL} = 0.4089101874\ J/m^2$, and $\delta_0 = 0.34$ nm is the equilibrium interfacial spacing. Substituting Eqs. (3) and (4) into Eqs. (1) and (2), the following nonlinear partial differential equations for the DWCNT are obtained:

$$E_iI_i\frac{\partial^4 w_i}{\partial x^4} + \rho_iA_i\frac{\partial^2 w_i}{\partial t^2} = \frac{E_iA_i}{L}\int_0^L\left[\frac{dZ}{dx}\frac{\partial w_i}{\partial x} + \frac{1}{2}\left(\frac{\partial w_i}{\partial x}\right)^2\right]dx\cdot\left(\frac{\partial^2 w_i}{\partial x^2} + \frac{d^2Z}{dx^2}\right) + p_1(w_o - w_i) + p_2(w_o - w_i)^3 \tag{6}$$

$$E_oI_o\frac{\partial^4 w_o}{\partial x^4} + \rho_oA_o\frac{\partial^2 w_o}{\partial t^2} = \frac{E_oA_o}{L}\int_0^L\left[\frac{dZ}{dx}\frac{\partial w_o}{\partial x} + \frac{1}{2}\left(\frac{\partial w_o}{\partial x}\right)^2\right]dx \times\left(\frac{\partial^2 w_o}{\partial x^2} + \frac{d^2Z}{dx^2}\right) - kw_o - p_1(w_o - w_i) - p_2(w_o - w_i)^3 \tag{7}$$

It is assumed that the waviness of the tubes, $Z(x)$, follow the first eigenfunction of the linear system, i.e., $Z(x) = e\cdot\phi_1(x)$, where $\phi_1(x)$ is the first eigenfunction of the linear CNT. For instance, $Z(x) = e\cdot\sin(\pi x/L)$ [40] for the case of simply supported tubes, where e is the amplitude of the initial waviness.

3. Generalized differential quadrature method

Generalized differential quadrature method (GDQM) approximates the derivatives of a function with respect to a spatial variable at a given discrete point by a weighted linear summation of function values at all the discrete points in the computational domain. For example, the nth derivative of a function $W_r(x)$ at the mth point, x_m, can be estimated by

$$W_r^{(n)}(x_m) = \sum_{s=1}^{N} c_{m,s}^{(n)}W_r(x_s), \quad m = 1,2,\ldots,N, \tag{8}$$

where $W_r^{(n)}(x_m)$ is the nth order derivative of $W_r(x)$ at point x_m, and N is the number of grid points utilized in the discretization of the partial derivatives. In Eq. (8) r refers to innertube or outertube, and $c_{m,s}^{(n)}(s = 1,\ldots,N)$ are the weighting coefficients for the nth derivative estimation of the mth point, which can be pre-determined [41]. Defining ${}_sW_r = W_r(x_s)$, Eq. (8) can be shorten as follows:

$${}_mW_r^{(n)} = \sum_{s=1}^{N} c_{m,ss}^{(n)}W_r, \quad j = 1,2,\ldots,N. \tag{9}$$

In the generalized differential quadrature method, the global Lagrange interpolation polynomial is used to calculate the weighting coefficients. Detailed information on how to obtain the weighting coefficients can be found in [42]. It is worth noting that higher order of weighting coefficients can be calculated by using matrix multiplication as follows:

$$\mathbf{C}^{(n)} = \mathbf{C}^{(n-1)}\mathbf{C}^{(1)} \tag{10}$$

where $\mathbf{C}^{(1)}$ is the matrix of weighting coefficients for the first derivative. Since the positions of the sampling points play a significant role in the accuracy of DQM [43], Gauss–Lobatto quadrature points, which result in minimum error, are used.

4. Application of DQM

A separable solution of $w_r(x,t) = W_r(x)\cdot T(t)$ is used in the partial differential equations of motions defined by Eqs. (6) and (7). Furthermore, assuming a single harmonic solution in time for the temporal part, i.e. utilizing harmonic balance method (HBM) with a single harmonic, and applying the GDQM, the following nonlinear algebraic equations of motion at the mth grid point are obtained

$$E_iI_i\left\{\sum_{s=1}^{N} c_{m,ss}^{(4)}W_i\right\} - \omega^2\rho_iA_{im}W_i = \frac{EA_i}{L}\left\{\sum_{n=1}^{N} d_n\left(\frac{dZ}{dx}\Big|_{x=x_n}\left\{\sum_{s=1}^{N} c_{n,ss}^{(1)}W_i\right\}\right)\right\}\frac{d^2Z}{dx^2}\Big|_{x=x_m} + \frac{3E_iA_i}{4L}\left\{\sum_{n=1}^{N} d_n\left(\frac{1}{2}\left\{\sum_{s=1}^{N} c_{n,s_s}W_i\right\}^2\right)\right\}\left\{\sum_{s=1}^{N} c_{m,ss}^{(2)}W_i\right\} + p_1({}_mW_o - {}_mW_i) + \frac{3p_2}{4}({}_mW_o - {}_mW_i)^3 \tag{11}$$

$$E_oI_o\left\{\sum_{s=1}^{N} c_{m,ss}^{(4)}W_o\right\} - \omega^2\rho_oA_{om}W_o = \frac{E_oA_o}{L}\left\{\sum_{n=1}^{N} d_n\left(\frac{dZ}{dx}\Big|_{x=x_n}\left\{\sum_{s=1}^{N} c_{n,ss}^{(1)}W_o\right\}\right)\right\}\frac{d^2Z}{dx^2}\Big|_{x=x_m} + \frac{3E_oA_o}{4L}\left\{\sum_{n=1}^{N} d_n\left(\frac{1}{2}\left\{\sum_{s=1}^{N} c_{n,s_s}W_o\right\}^2\right)\right\}\left\{\sum_{s=1}^{N} c_{m,ss}^{(2)}W_o\right\} - p_1({}_mW_o - {}_mW_i) - \frac{3p_2}{4}({}_mW_o - {}_mW_i)^3 - k_mW_o \tag{12}$$

where d_n is the weighting function which is calculated using Gauss–Lobatto integration rule. According to quadrature integration rule, integration value can be stated as a weighted sum of function values at specified points within the domain of integration as follows:

$$\int_a^b f(x)dx \simeq \frac{b-a}{2}\left(d_1\cdot f(a) + d_n\cdot f(b) + \sum_{i=2}^{n-1} d_i f\left(\frac{b-a}{2}z_i + \frac{b+a}{2}\right)\right), \tag{13}$$

$$d_i = \begin{cases} \frac{2}{n(n-1)[P_{n-1}(z_i)]^2}, & 2\le i\le n-1 \\ \frac{2}{n(n-1)}, & i = 1,n \end{cases} \tag{14}$$

where $P_n(z)$ is the nth order Legendre polynomial. The evaluation points are the roots of a polynomial belonging to a class of orthogonal polynomials which, in our case, is Gauss–Lobatto points. It is worth noting that the Gauss–Lobatto rule is accurate for polynomials up to the degree of $2n-3$, where n is the number of integration points [44]. Eqs. (11) and (12) can be written in matrix form for all the points as follows:

$$(\mathbf{K_L} + \mathbf{K_{NL}})\cdot\mathbf{x} - \omega^2\mathbf{M}\cdot\mathbf{x} = \mathbf{0}, \tag{15}$$

$$\mathbf{K_{NL}} = \mathbf{K_{NLg}} + \mathbf{K_{NLv}}, \tag{16}$$

where $\mathbf{x}$ denotes the unknown dynamic displacement vector defined as

$$\mathbf{x} = \{\,{}_1W_{i\,2}W_i\cdots{}_NW_{i\,1}W_{o\,2}W_o\cdots{}_NW_o\,\}^T, \tag{17}$$

and $\mathbf{M}$, $\mathbf{K_L}$, $\mathbf{K_{NLg}}$, and $\mathbf{K_{NLv}}$ represent mass matrix, linear stiffness matrix, and nonlinear stiffness matrices associated with geometric and vdW force nonlinearities of the system, respectively. These matrices are defined as

$$\mathbf{M}_{2N\times 2N} = identity \tag{18}$$

$$\mathbf{K_L} = \begin{bmatrix} \frac{E_i I_i}{\rho_i A_i}\cdot\mathbf{C}^{(4)} + \frac{p_1}{\rho_i A_i}\cdot\mathbf{I} - \frac{E_i e^2}{\rho_i L}\cdot\mathbf{E} & -\frac{p_1}{\rho_i A_i}\cdot\mathbf{I} \\ -\frac{p_1}{\rho_o A_o}\cdot\mathbf{I} & \frac{E_o I_o}{\rho_o A_o}\cdot\mathbf{C}^{(4)} + \frac{(p_1+k)}{\rho_o A_o}\cdot\mathbf{I} - \frac{E_o e^2}{\rho_o L}\cdot\mathbf{E} \end{bmatrix}, \tag{19}$$

$$\mathbf{K_{NLg}} = \frac{3}{4L}\cdot\begin{bmatrix} \beta_i \frac{E_i}{\rho_i}\mathbf{C}^{(2)} & [0] \\ [0] & \beta_o \frac{E_o}{\rho_o}\mathbf{C}^{(2)} \end{bmatrix}, \tag{20}$$

$$\mathbf{K_{NLv}} = \frac{3p_2}{4}\begin{bmatrix} \frac{1}{\rho_i A_i}[\mathbf{K}_1 \quad \mathbf{K}_2] \\ \frac{-1}{\rho_o A_o}[\mathbf{K}_1 \quad \mathbf{K}_2] \end{bmatrix}. \tag{21}$$

$\mathbf{I}$ is identity matrix, $\mathbf{C}^{(n)}$ indicates weighting function matrix for the nth order derivative using DQM, $\mathbf{E}$ stands for initial waviness matrix, $\beta_r (r = i,\ o)$ is a displacement dependent coefficient representing geometric nonlinearity, and $\mathbf{K}_1$ and $\mathbf{K}_2$ are displacement dependent matrices which are given in Appendix A.

In the present study, three common sets of boundary conditions namely as hinged–hinged (H–H), clamped–hinged (C–H), and clamped–clamped (C–C) are investigated. Boundary conditions for hinged and clamped ends are

$$w_r(x_s, t) = 0, \quad \left.\frac{d^2 w_r}{dx^2}\right|_{x = x_s} = 0, \tag{22}$$

$$w_r(x_s, t) = 0, \quad \left.\frac{dw_r}{dx^2}\right|_{x = x_s} = 0, \tag{23}$$

respectively. Where $s = 1$ and $s = N$ represents the end points. Using the GDQM, the discretized counterparts of different boundary conditions given by Eqs. (22) and (23) can be written in matrix form as follows:

$$\begin{bmatrix} 1 & 0 & \cdots & 0 & 0 & & \\ c_{1,1}^{(n_L)} & c_{1,2}^{(n_L)} & \cdots & c_{1,N-1}^{(n_L)} & c_{1,N}^{(n_L)} & & [0] \\ c_{N,1}^{(n_R)} & c_{N,2}^{(n_R)} & \cdots & c_{N,N-1}^{(n_R)} & c_{N,N}^{(n_R)} & & \\ 0 & 0 & \cdots & 0 & 1 & & \\ & [0] & & & & \begin{matrix} 1 & 0 & \cdots & 0 & 0 \\ c_{1,1}^{(n_L)} & c_{1,2}^{(n_L)} & \cdots & c_{1,N-1}^{(n_L)} & c_{1,N}^{(n_L)} \\ c_{N,1}^{(n_R)} & c_{N,2}^{(n_R)} & \cdots & c_{N,N-1}^{(n_R)} & c_{N,N}^{(n_R)} \\ 0 & 0 & \cdots & 0 & 1 \end{matrix} \end{bmatrix}_{8\times 2N}$$

$$\{ {}_1W_{i2}W_i \vdots_{N-1} W_{iN}W_{i1}W_{o2}W_o \vdots_{N-1} W_{oN}W_o \}_{2N\times 1} = \{0\}. \tag{24}$$

Superscripts n_L and n_R are assigned by the type of the left and the right end conditions, where they are equal to 1 for the clamped end and 2 for the hinged end. By using matrix manipulation Eq. (24) can be written as

$$\mathbf{K_B}\cdot\mathbf{x_s} + \mathbf{K_S}\cdot\mathbf{x}^* = \mathbf{0}, \tag{25}$$

where

$$\mathbf{x_s} = \{ {}_1W_{i,2}W_{i,N-1}W_{i,N}W_1W_{o,2}W_{o,N-1}W_{o,N}W_o \}^T, \tag{26}$$

$$\mathbf{x}^* = \{ {}_3W_{i4}W_i \cdots_{N-2} W_{i3}W_{o4}W_o \cdots_{N-2} W_o \}^T. \tag{27}$$

representing boundary and interior nodes and $\mathbf{K_B}$ and $\mathbf{K_S}$ are 8×8 and $8\times(2N-8)$ matrices related with boundary and interior nodes, respectively. Following a similar approach Eq. (15) can be written as

$$\mathbf{K_D}\cdot\mathbf{x_s} + (\mathbf{K}_\mathbf{L}^* + \mathbf{K}_\mathbf{NL}^*)\cdot\mathbf{x}^* - \omega^2\mathbf{M}^*\cdot\mathbf{x}^* = \mathbf{0} \tag{28}$$

Here $\mathbf{K}_\mathbf{L}^*$, $\mathbf{K}_\mathbf{NL}^*$, and $\mathbf{M}^*$ are $(2N-8)\times(2N-8)$ matrices, representing the linear stiffness matrix, nonlinear stiffness matrix, and mass matrix for the interior nodes, respectively. It is worth noting that $\mathbf{K}_\mathbf{L}^*$, $\mathbf{K}_\mathbf{NL}^*$, and $\mathbf{M}^*$are coefficient matrices for the non-boundary nodes, where $\mathbf{K}_\mathbf{NL}^*$ is a displacement dependent matrix whose values depend on the values of the boundary nodes in addition to the interior nodes. $\mathbf{K_D}$ is an $(2N-8)\times 8$ matrix, which contains coefficient of boundary nodes.

Solving $\mathbf{x_s}$ from Eq. (25) and substituting it in Eq. (28), equation of motion of the system is obtained as follows:

$$[(\mathbf{K}_\mathbf{L}^* + \mathbf{K}_\mathbf{NL}^*) - \mathbf{K_D}\mathbf{K_B}^{-1}\mathbf{K_S}]\cdot\mathbf{x}^* = \omega^2\mathbf{M}^*\cdot\mathbf{x}^* \tag{29}$$

5. Solution method

The set of nonlinear algebraic equations given by Eq. (29) can be solved numerically by using Newton's method with Arc-length continuation. Newton's method converges to the correct solution quadratically, if the initial guess is sufficiently close to the actual solution. However, convergence problems arise when a solution is around a turning point since the Jacobian matrix becomes singular. Moreover, in order to follow the solution branch even it reverses its direction; continuation parameter has to be replaced with another parameter for which it is possible to follow the path (arc-length continuation). Details of Newton's method with arc-length continuation can be found in [19].

Another solution approach commonly used by a number of researchers is a direct iterative process (DIP) by using eigenvalue solvers. In this method [26,45], vibration amplitude increases incrementally. At each step, nonlinear vibration dependent stiffness matrices are calculated based on the mode shape of the previous solution. The resultant linear system can be solved using an eigenvalue solver. This process is repeated until the difference between the assumed and calculated eigenmodes decreases to a predetermined tolerance. It should be noted that DIP method is established based on the assumption that variation of mode shapes along the solution path is small. However, due to strong nonlinearities existing in the problem, nonlinear system mode shape changes significantly along the solution path as shown in [19], where DIP fails in finding the correct solution and therefore it cannot be used directly. Moreover, the effect of each nonlinearity is different whether the in-phase vibration mode or out-of-phase vibration mode is considered. For example, due to vdW force nonlinearity out-of-phase natural frequencies increase significantly as the maximum vibration amplitude increases; whereas, in-phase natural frequencies change slightly with respect to the maximum vibration amplitude. As a result of this, it is possible for the path of system natural frequencies to cross each other as presented in [19]. For instance, system can vibrate in the second mode (out-of-phase mode) with a nonlinear natural frequency higher than the nonlinear natural frequency of the third mode (in-phase mode) as vibration amplitude increases. Hence, in the present study, in order to overcome these two problems, a new method referred as "iterative path following method" is developed, which combines modal assurance criterion (MAC) and arc-length continuation method with DIP in order to improve its performance. In the iterative path following method (IPFM), by utilizing MAC it is possible to track the correct natural frequency and by using arc-length continuation it is possible to follow the solution path in the presence of multiple solutions.

The modal assurance criterion is outlined as a scalar constant relating the degree of consistency (linearity) between two vectors as follows:

$$MAC = \frac{|\{\psi_A\}^T\{\psi_X\}|^2}{|\{\psi_A\}^T\{\psi_A\}||\{\psi_X\}^T\{\psi_X\}|}, \tag{30}$$

where $\{\psi_A\}$ and $\{\psi_x\}$ are two vectors that are compared with each other. The modal assurance criterion takes values between 0 and 1, where 0 and 1 indicate two independent and identical vectors, respectively. Thus, if the modal vectors under study truly express a consistent, linear relationship, the modal assurance criterion approaches unity. This fact is utilized in finding the system eigenvalues. Additionally, instead of increasing incrementally the vibration amplitude, which may result in jump up or down in case of multiple solutions, arc-length continuation is utilized to follow the solution branch around turning points, in which the maximum vibration amplitude becomes an unknown and arc-length is the parameter used in path following.

The solution method consists of two major loops the arc-length loop and direct iterative process loop which acts inside the arc-length loop. The step by step description of the developed iterative path following method (IPFM) is given as follows:

Step 1: The nonlinear equation of motion given in Eq. (29) can be written as a residual vector function as

$$\mathbf{f}(\mathbf{x}^*,\omega)=\{(\mathbf{K}_\mathbf{L}^*+\mathbf{K}_\mathbf{NL}^*)-\mathbf{K}_\mathbf{D}\mathbf{K}_\mathbf{B}^{-1}\mathbf{K}_\mathbf{S}\}\cdot\mathbf{x}^*-\omega^2\mathbf{M}^*\cdot\mathbf{x}^*=0, \tag{31}$$

$$\mathbf{x}^*=W_{\max}\cdot\left\{\ {}_3\tilde{W}_{i\,4}\tilde{W}_i\cdots_{N-2}\tilde{W}_{i\,3}\tilde{W}_{o\,4}\tilde{W}_o\cdots_{N-2}\tilde{W}_o\right\}^T=W_{\max}\tilde{\mathbf{x}}^*, \tag{32}$$

where ${}_k\tilde{W}_i$ and ${}_k\tilde{W}_o$ represent the normalized vibration amplitudes of the mode shapes of inner and outer tubes with respect to the grid point of the innertube or outertube that result in the maximum absolute value. The arc length parameter is defined as the radius of a fictitious n-dimensional sphere centered at the previous converged solution point. It should be noted that in the first step, linear system eigenvector is considered as the reference mode. The new solution will be searched on the surface of this sphere rather than at the next vibration amplitude, where the amplitude become an unknown and the radius of the fictitious sphere is the parameter specified. Details about applying the arc-length method to a residual function can be found in [19]. Arc-length continuation is used to update the mode shapes obtained in the previous solution and predict the next vibration amplitude.

Step 2: DIP loop starts here, where calculated eigenvectors are used to determine the nonlinear stiffness matrix, $\mathbf{K}_\mathbf{NL}^*$, and new eigenvalues and eigenvectors are calculated from the updated eigensystem. MAC is calculated based on the eigenvector of previous solution in order to select the correct eigenvector and the eigenvalue associated with it.

Step 3: The calculated eigenvector is normalized and step 2 is repeated until the error in the residual function given by Eq. (31) is within predefined tolerance limit.

It should be noted that the maximum vibration amplitude does not occur at the same point on the CNTs; moreover, it can occur at points other than DQM points. Hence, in order to find the maximum vibration amplitude, after obtaining the nonlinear eigenvector, the full mode shape is reconstructed using Lagrange interpolation and the point of maximum amplitude is determined.

6. Results

In the following section, the effect of nonlinearities on the first in-phase and out-of-phase fundamental natural frequencies of a curved DWCNT is investigated. Firstly, the effect of geometric nonlinearity and initial curvature on the nonlinear natural frequency of a DWCNT is studied by presenting the variation of normalized nonlinear natural frequency with respect to the maximum vibration amplitude. Later, the same study is repeated considering the effect of vdW force nonlinearity together with the geometric nonlinearity. Finally, considering both nonlinearities medium stiffness on the nonlinear natural frequency of the DWCNTs are investigated. Meanwhile, the effects of different end conditions are as well considered in the studies performed. In order to present the results in a proper form, the nonlinear natural frequency is normalized with respect to the corresponding linear natural frequency of the curved DWCNT and vibration amplitudes are normalized with respect to $\sqrt{I_i/A_i}$.

The numerical values of the parameters used in this study are given in Table 1. Before proceeding into the nonlinear analysis, the effect of number of grid points is studied on the linear system, where it is observed that the natural frequencies obtained for all types of boundary conditions considered are identical in case the number of grid points is larger or equal to 13. Therefore, in all the results presented, 18 grid points are utilized which is observed to be sufficient for the nonlinear cases as well. These results are not presented here for brevity.

In Table 2, the fundamental natural frequency of the linear DWCNT with H–H end conditions are compared with the analytical solution and the results given in literature. It can be seen that the results of DQM and analytical solution are in very good agreement.

6.1. Effect of geometric nonlinearity and initial curvature

In Fig. 2, the variation of the normalized nonlinear natural frequency of the first in-phase vibration mode of a DWCNT is given for hinged–hinged, clamped–hinged, and clamped–clamped boundary conditions with different values of initial curvature (waviness) in the presence of only geometric nonlinearity. A hardening stiffness behavior is observed for all types of boundary conditions, i.e. the nonlinear natural frequency increases as the vibration amplitude increases. Furthermore, it is observed that although the clamped–clamped DWCNT have the highest fundamental linear natural frequencies, it has the lowest normalized nonlinear natural frequency at the same maximum vibration amplitude. This is an expected result, since the effect of geometric nonlinearity decreases due to the limited deformation obtained for stronger end supports. Furthermore, it is observed that, for all the cases, normalized nonlinear natural frequency decreases as waviness increases and tends to approach to the linear one. Moreover, it can be seen that as the end conditions get stronger, the effect of

Table 1
Numerical values of tubes parameters.

Parameter	Value
Innertube diameter	$d_i=0.7$ nm
Outertube diameter	$d_0=1.4$ nm
Young's modulus	$E=1$ TPa
Poisson's ratio	$\nu=0.25$
Thickness of each tube	$t=0.34$ nm

Table 2
Fundamental Linear Natural Frequencies of a Simply Supported DWCNT.

Natural frequencies	In-phase	Out-of-phase
Ref. [19]	0.4673	7.8852
Ref. [17]	0.46	7.71
Analytical solution	0.467289	7.885189
Present study, DQM	0.467289	7.885189

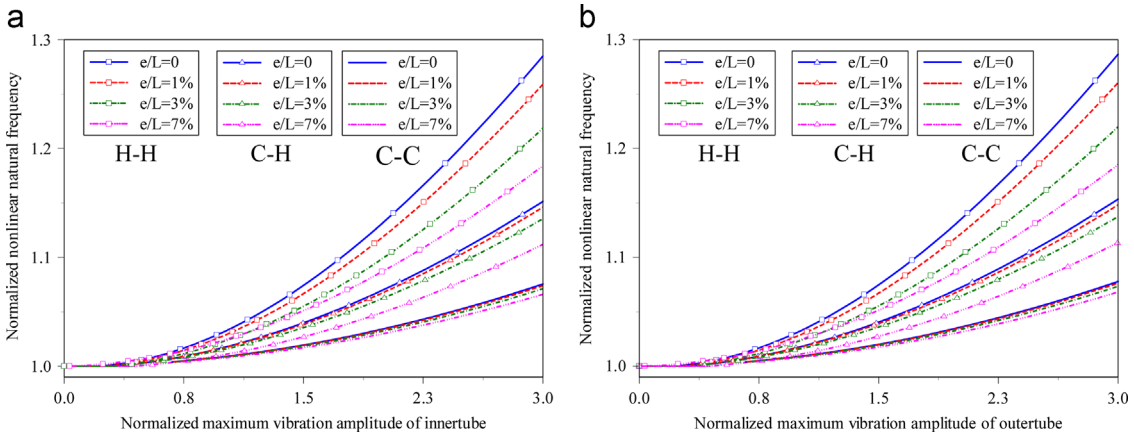

Fig. 2. Variation of normalized nonlinear natural frequency of inner and outer tubes vibrating in the first in-phase mode for different end conditions and initial curvature.

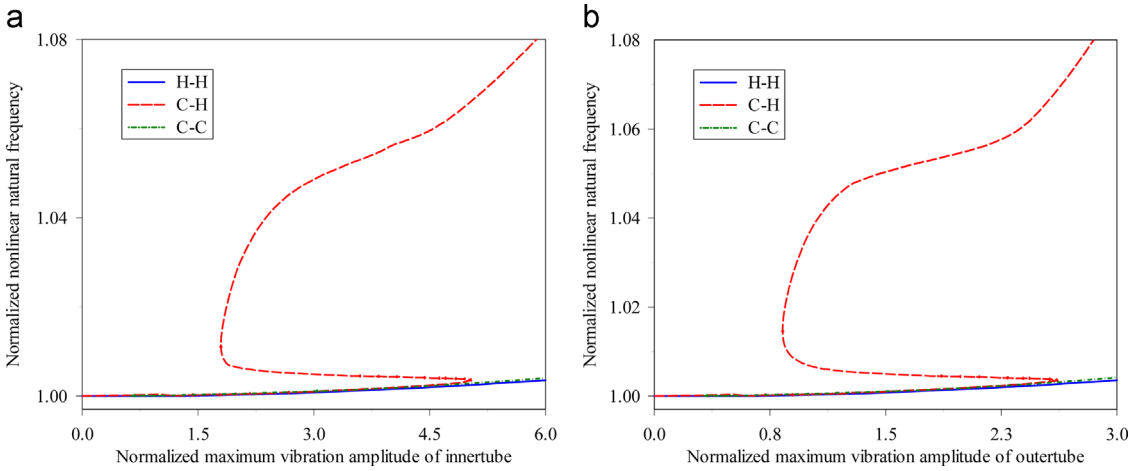

Fig. 3. Variation of normalized nonlinear natural frequency of inner and outer tubes vibrating in the first out-of-phase mode for different end conditions ($e=0$)

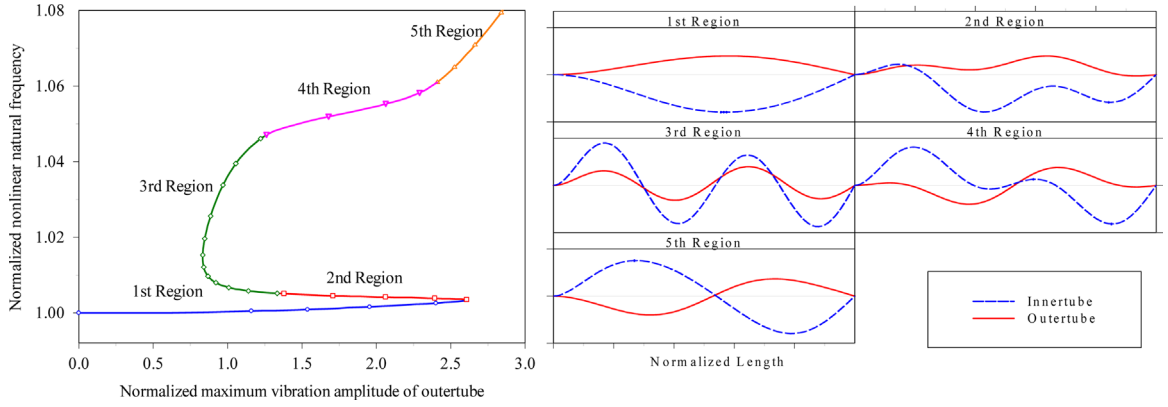

Fig. 4. Variation of normalized nonlinear natural frequency of outertube vibrating in the first out-of-phase mode and the corresponding mode shapes in the middle of each region.

initial curvature on the variation of nonlinear natural frequency decreases.

Fig. 3 shows the variation of the normalized nonlinear natural frequency of a DWCNT vibrating in the first out-of-phase vibration mode where the effect of different boundary conditions is investigated. It should be noted that the effect of initial curvature is insignificant for the case of out-of-phase vibration mode; hence, for brevity, those results are not presented here. Furthermore, for clarity, initial curvature is considered to be equal to zero in the cases of out-of-phase vibration modes presented in this study. Results show that in contrast to in-phase vibration mode, the variation of nonlinear natural frequency increases as end conditions get stronger for the out-of-phase vibration mode. However, the amount of the increase in the nonlinear natural frequency is lower than the case of in-phase vibration mode and for H–H and C–C boundary conditions, it is negligible. Moreover, several turning points are observed for C–H end conditions, where at a single vibration amplitude multiple nonlinear natural frequencies exist.

In Fig. 4, the variation of nonlinear natural frequency for the C–H end conditions is re-plotted by dividing the plot into five regions where the corresponding mode shapes of the tubes at the center of each region is given as well. The regions are defined by considering the changes in the characteristics of the nonlinear mode shape, where, for some cases, it occurs around turning points. It can be seen that in the first region, the system vibrates in a mode shape similar to the fundamental out-of-phase mode shape of the linear system. However as the region number increases, the contribution of other linear modes become significant in the nonlinear solution. For instance, in the second region the system vibrates in a mode shape which can be identified as a combination of the first out-of-phase and the fourth in-phase linear vibration modes. In order to clearly study the contribution of each linear vibration mode to the nonlinear solution, variation of normalized modal contributions along the solution curve is plotted in Fig. 5 for the first six modes that have the highest contributions. Normalized modal contributions are calculated using Eq. (30), where the nonlinear mode shape is compared with the linear modes of corresponding system. It can be seen that moving forward along the solution curve the contribution of the first out-of- phase mode decreases and at the same time the contribution of the forth in-phase mode increases and becomes maximum in the middle of the third region. Proceeding further, contribution of the fourth in-phase mode decreases; whereas, the contribution of the second out-of-phase mode starts to increase and dominates the nonlinear solution. Our further studies show that system continues to vibrate in the second out-of-phase mode and does not return to the first out-of-phase vibration mode as vibration amplitude increases. This is due to the fact that, in the path following method, the nonlinear vibration mode which is closer to the one at the previous amplitude step is followed; however, for H–H and C–C boundary conditions, which are symmetric, the first out-of-phase vibration mode is dominant in the nonlinear vibration mode.

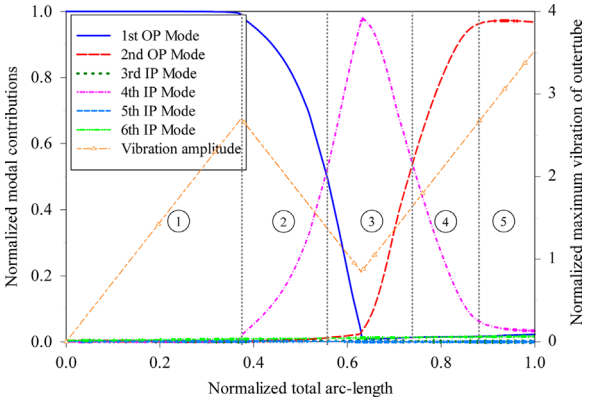

Fig. 5. Variation of normalized modal contributions vs. normalized total arc-length.

6.2. *Van der Waals force nonlinearity together with geometric nonlinearity*

The variation of normalized nonlinear natural frequency in the first in-phase vibration mode is studied in the presence of both

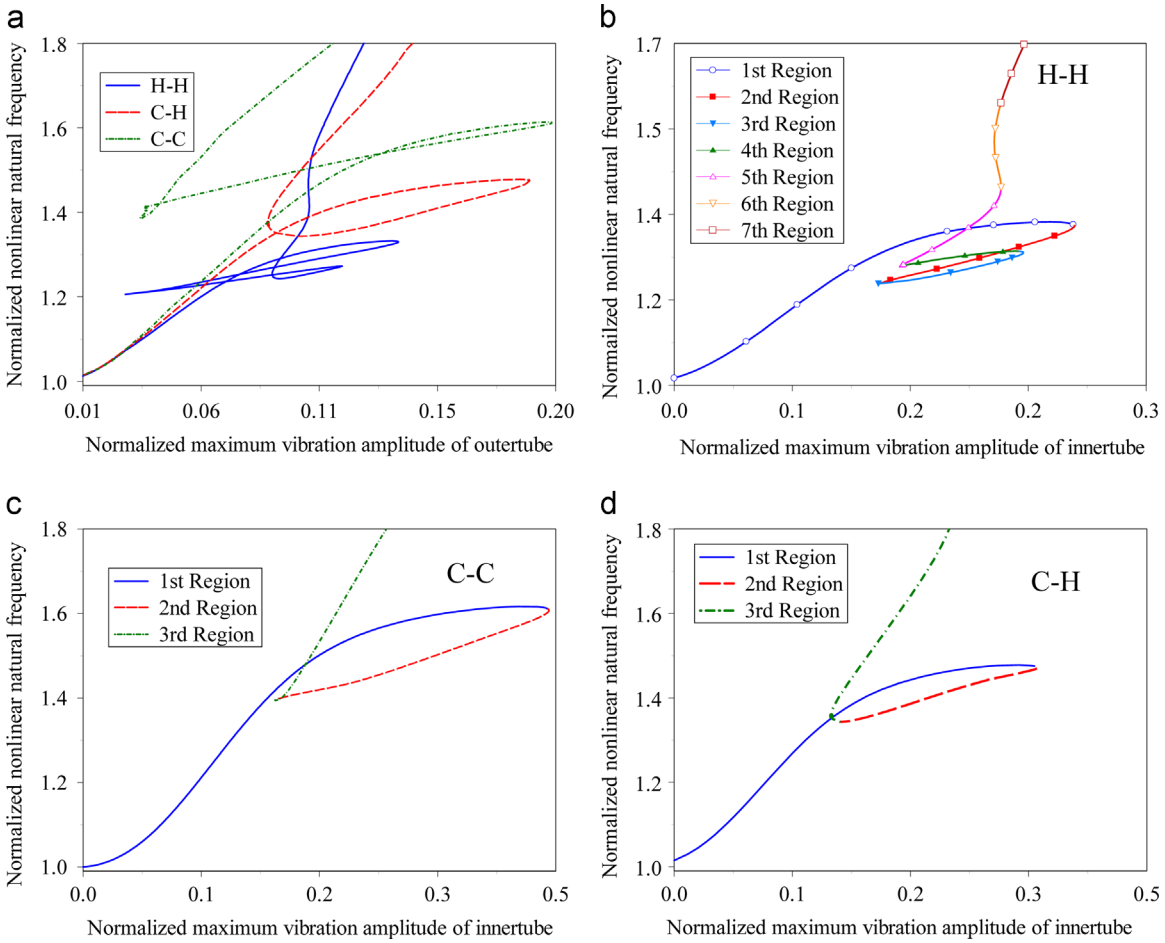

Fig. 6. Variation of normalized nonlinear natural frequency of DWCNT vibrating in the first out-of-phase mode (a) Comparison of all end conditions in the presence of both vdW force and geometric nonlinearities, (b) H–H, (c) C–H, and (d) C–C.

geometric and vdW force nonlinearities for different types of end conditions and initial curvature. It is observed that in the in-phase vibration mode, nonlinear natural frequency majorly changes due to geometric nonlinearity and considering the vdW force nonlinearity in addition to geometric nonlinearity does not affect the vibratory behavior of the DWCNT; hence, results very similar to the ones given in Fig. 2 is obtained. Therefore, for brevity these results are not presented here. This is an expected result, since vdW force nonlinearity depends on the relative motion between the inner and outer tubes and in the in-phase vibration modes, relative motion between the tubes changes slightly during free vibration.

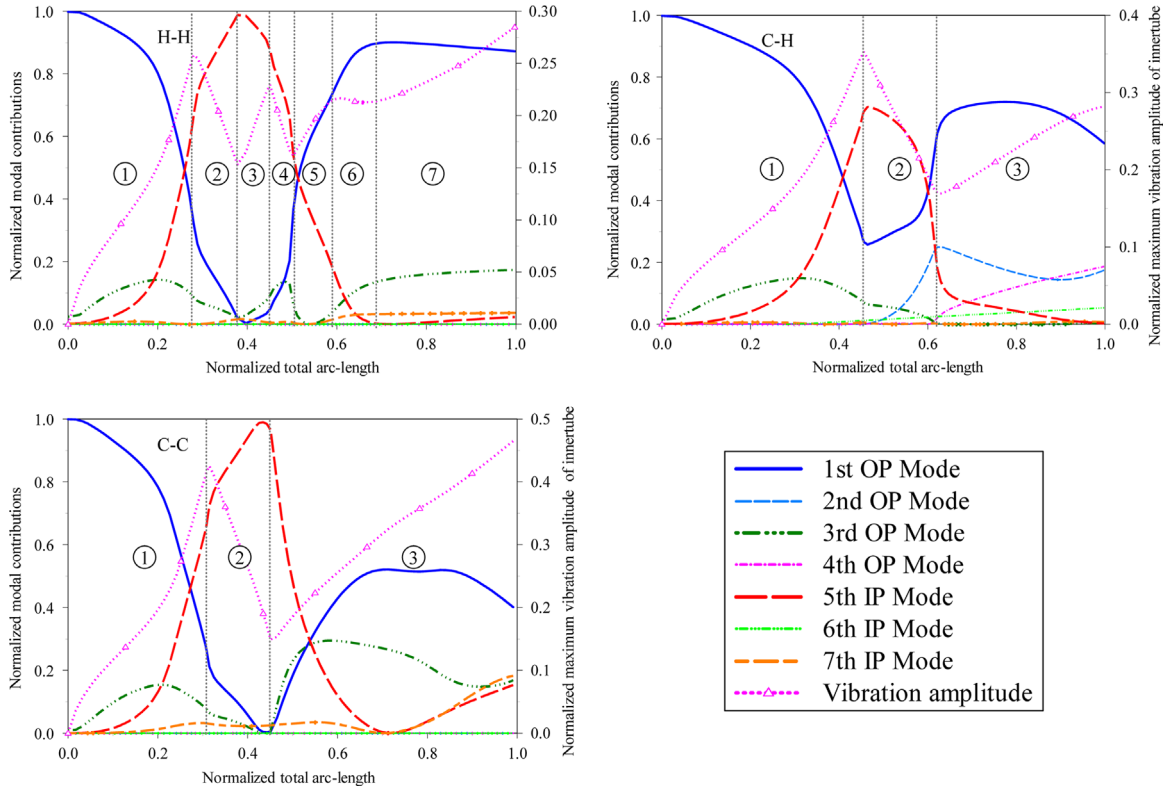

Fig. 7. Variation of normalized modal contributions vs. total arc-length (a) H–H, (b) C–H, and (c) C–C.

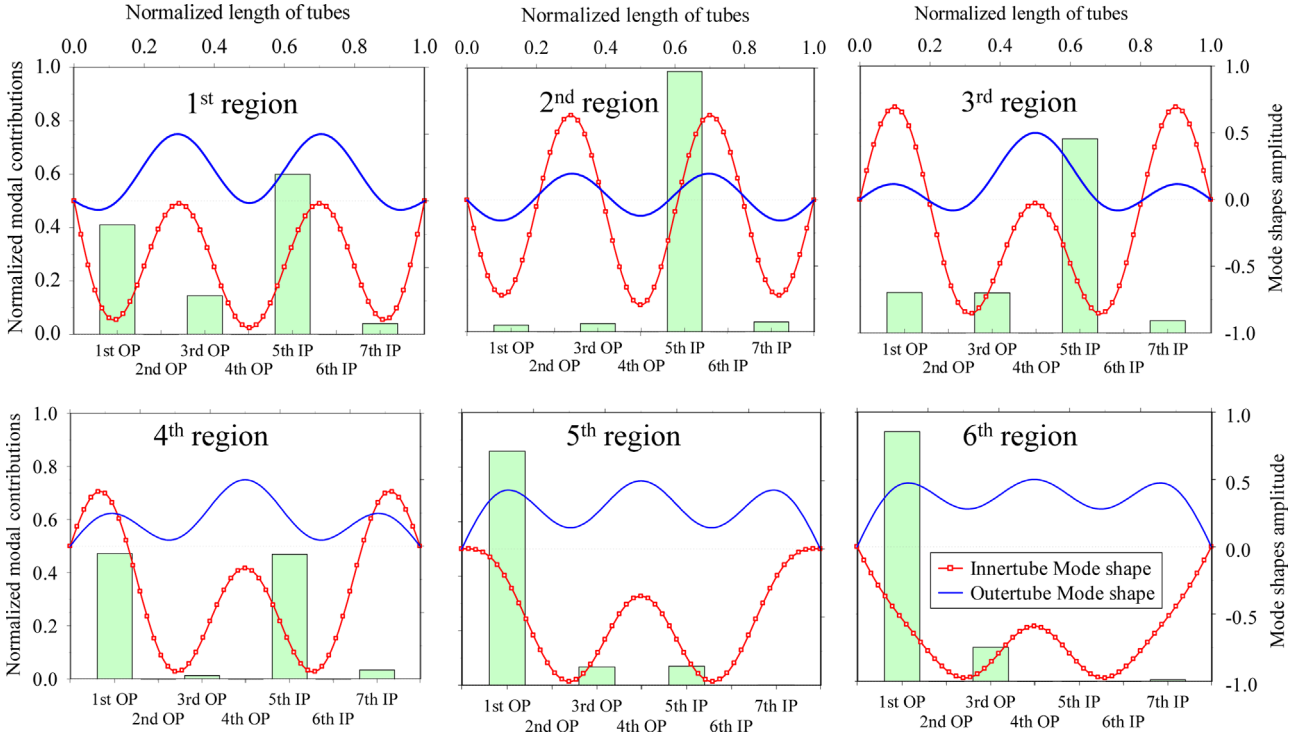

Fig. 8. Normalized modal contribution of innertube and the mode shapes of inner and outer tubes at the end of each region for H–H DWCNT.

Fig. 6a shows the variation of the normalized nonlinear natural frequency for the case of the first out-of-phase vibration mode considering different types of end conditions. Results show that due to the vdW force nonlinearity, nonlinear natural frequency changes considerably where several turning points are observed for all end conditions considered. The results obtained for the H–H DWCNT are the same as the ones presented by Cigeroglu and Samandari [19], where authors used a Galerkin based discretization method. In Fig. 6c, b, and d, variation of the normalized nonlinear natural frequency for each end condition is given, where the curves are divided into seven different regions indicated by different markers and colors. In Fig. 7, variation of the normalized contribution of each linear mode shape is plotted for the first seven modes that have the highest contributions, where different regions are indicated by numbers. It can be seen that for all the cases as total arc-length increases, or as the region number increases, the contribution of the first linear out-of-phase mode decreases and later increases again. Moreover, it is observed that for all the cases in the region for which the contribution of the first mode becomes a minimum (2nd region for C–C and C–H, and 2nd–4th regions for H–H), CNTs vibrate as if it is vibrating in the fifth linear in-phase mode.

Fig. 8 shows a bar plot of normalized modal contributions of the system for H–H DWCNT at the end of each region, shown in Fig. 6, in addition to the corresponding nonlinear mode shapes of the inner and outer tubes. It can be seen that at the end of the first region CNTs vibrate in a nonlinear mode shape completely different from the first linear out-of-phase mode shape where the contribution of the fifth in-phase mode passes the contribution of the first out-of-phase mode. It can be seen that at the end of the 2nd region, the contribution of the fifth in-phase mode reaches to its maximum, which starts to decrease and become zero at the end of the sixth region. It is worth noting that for the case of H–H DWCNT only the odd mode shapes are excited which verifies the results given in [19].

In Fig. 9, normalized modal contribution of C–H DWCNT is given around the middle of each region in addition to the corresponding nonlinear mode shapes of the inner and outer tubes. It is observed that for the case of C–H DWCNT, in addition to odd modes, even modes are also excited. Moreover, it can be seen that asymmetric boundaries resulted in asymmetric mode shapes. Fig. 10 shows a similar plot for C–C DWCNT. It is observed that, for the present case, only the odd modes are excited. Therefore, it can be concluded that for symmetric boundary conditions only the odd mode shapes are present in the nonlinear modes whereas for

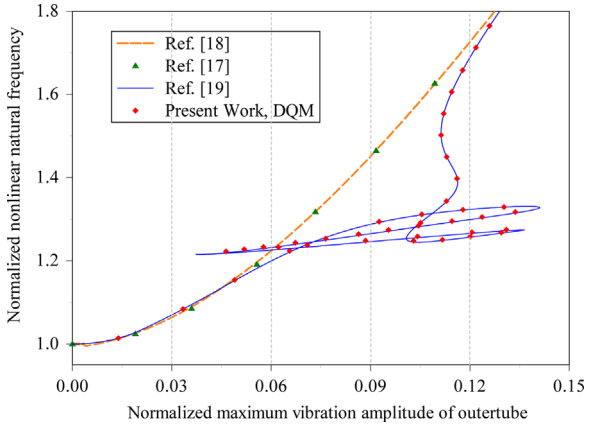

Fig. 11. Comparison with available data in the literature for a H–H DWCNT.

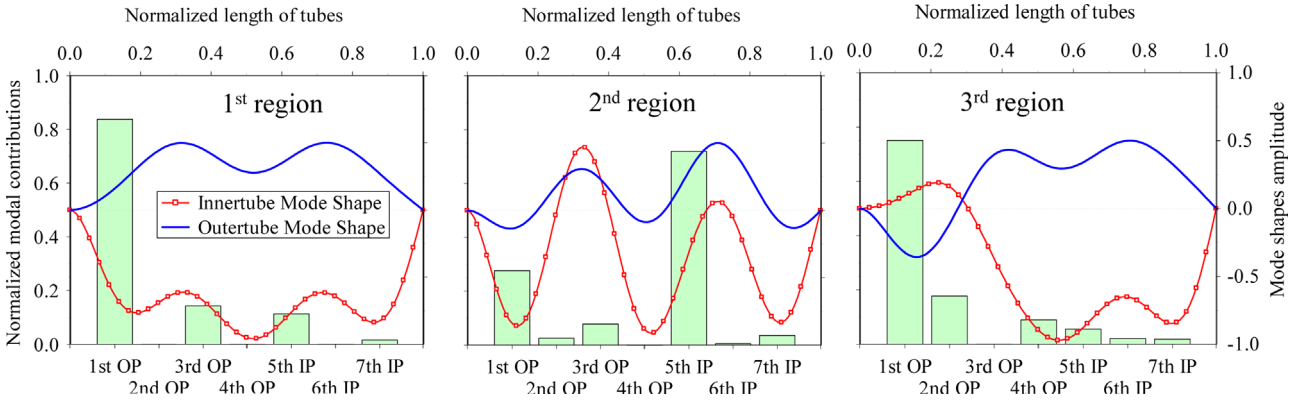

Fig. 9. Normalized modal contributions of innertube and the mode shapes of inner and outer tubes around the middle of each region for C–H DWCNT.

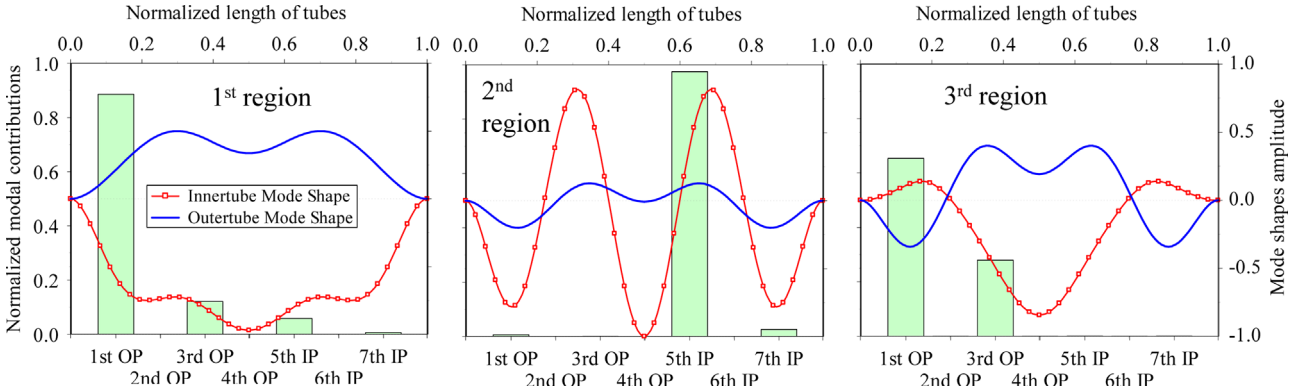

Fig. 10. Normalized modal contributions of innertube and the mode shapes of inner and outer tubes around the middle of each region for C–C DWCNT.

asymmetrical end conditions in addition to the odd modes, even modes as well contribute to the nonlinear mode shapes.

Fig. 11 represents a comparison between the results of current study and available results in the literature. It is observed that the solutions obtained in the present study by utilizing DQM and the results given in literature by using multiple trail function and Galerkin method [19] are in good agreement. For the case of H–H DWCNT, the results at selected points obtained by the present study (DQM) and by Galerkin method [19] are tabulated in Table 3. It observed that both results are in good agreement and slight differences between the values are due to the nature of the two different methods compared.

6.3. Effect of medium stiffness

Fig. 12 presents the effect of the medium stiffness, k, on the variation of normalized nonlinear natural frequency versus maximum vibration amplitude for H–H, C–H, and C–C DWCNT. It is observed that with an increase in the medium stiffness, k, the normalized nonlinear frequency tends to approach to the linear one for all end conditions. It is seen that for H–H end condition with medium stiffness less than 10^8 N/m^2, variation of normalized nonlinear natural frequency changes slightly; whereas, for medium stiffness larger than 10^8 N/m^2 significant changes in the normalized nonlinear natural frequency are observed. A similar behavior is observed formerly for variation of linear natural frequencies. This shows that the effect of geometric nonlinearity becomes negligible in the presence of sufficiently large medium stiffness. Moreover, it is observed that as boundary conditions get stiffer in addition to decreasing in variation of nonlinear natural frequency, the threshold value of medium stiffness increases. The results are tabulated in Table 4. A similar behavior is detected for the case of out-of-phase vibration modes therefore for brevity it is not presented here. The results for the case of H–H DWCT vibrating in the first out of phase vibration mode can be found in [19].

7. Conclusion

In this paper, nonlinear free vibration of a curved DWCNT embedded in elastic medium is studied by using differential quadrature method (DQM) where in addition to geometric nonlinearity, interlayer vdW force nonlinearity is also included. The effect of nonlinearities, end conditions, initial curvature, stiffness

Table 3
DQM and Galerkin results at selected points for a H–H DWCNT.

Normalized maximum vibration amplitude	0.03	0.06	0.09	0.12
Normalized nonlinear natural frequency (present study, DQM)	1.0700	1.2022, 1.2314, 1.2355	1.2496, 1.2682, 1.2891	1.2583, 1.2682, 1.3011, 1.3242, 1.6890
Normalized nonlinear natural frequency (Galerkin) [19]	1.0700	1.1995, 1.2258, 1.2317	1.2460, 1.2652, 1.2875	1.2568, 1.2659, 1.2989, 1.3235, 1.6885

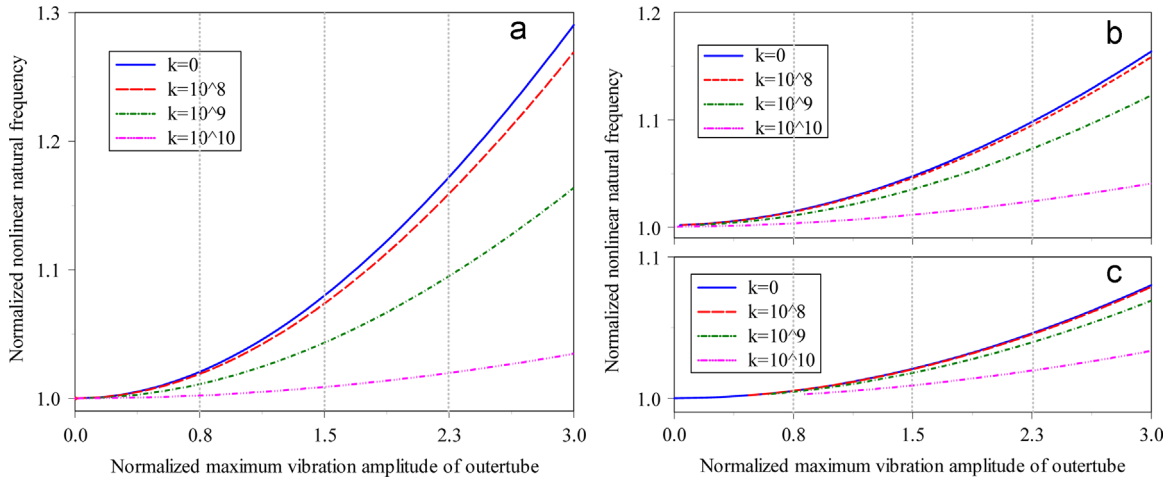

Fig. 12. Effect of medium stiffness on the nonlinear fundamental natural frequency of DWCNT vibrating in the first in-phase vibration mode (a) hinged–hinged, (b) clamped–hinged, and (c) clamped–clamped ($e=0$)

Table 4
Normalized nonlinear natural frequencies at selected normalized vibration amplitudes of outertube.

Normalized vibration amplitude of outertube	Normalized nonlinear natural frequency											
	H–H Medium stiffness				C–H Medium stiffness				C–C Medium stiffness			
	0	10^8	10^9	10^{10}	0	10^8	10^9	10^{10}	0	10^8	10^9	10^{10}
0.8	1.0234	1.0216	1.0126	1.0025	1.0162	1.0156	1.0119	1.0039	1.0060	1.0059	1.0052	1.0025
1.5	1.0799	1.0736	1.0434	1.0089	1.0473	1.0457	1.0351	1.0115	1.0208	1.0204	1.0178	1.0091
2.3	1.1793	1.1658	1.0992	1.0206	1.1019	1.0985	1.0759	1.0251	1.0480	1.0472	1.0412	1.0203

of the surrounding elastic medium, and vibrational modes on the nonlinear free vibration of DWCNTs is studied in detail.

Results show that nonlinear natural frequency increases as vibration amplitude increases in the presence of only geometric nonlinearity for all the type of end conditions. Moreover, it is observed that multiple solution at same vibration amplitude can exist due to interaction of nonlinear in-phase and out-of-phase vibration modes.

Furthermore, application of DQM made it possible for the first time to study the effect of different boundary conditions in the presence of vdW force nonlinearity on the variation of the nonlinear natural frequencies of DWCNTs. Results show that due to the vdW force nonlinearity, nonlinear natural frequency changes considerably where several turning points are as well observed. It is been observed that the number of turning points is different for each boundary condition considered. Moreover, it is observed that for symmetric boundary conditions only the odd mode shapes are present in the nonlinear modes whereas for asymmetrical end conditions in addition to the odd modes, even modes as well contribute to the nonlinear mode shapes.

Acknowledgments

Authors would like to gratefully acknowledge the partial support provided by the TUBITAK (The Scientific and Technological Research Council of Turkey), Grant no: 2215 – Graduate Scholarship Program for International Students.

Appendix A.

The initial waviness matrix given in Eq. (19) is defined as follows:

$$\mathbf{E}=\left\{\sum_{n=1}^{N} d_n\left(\phi'(x_n)\left\{\sum_{s=1}^{N} c_{n,ss}^{(1)} W_o\right\}\right)\right\} \times\begin{bmatrix}\phi''(x_3) & & & 0\\ & \phi''(x_4) & & \\ & & \ddots & \\ 0 & & & \phi''(x_{N-2})\end{bmatrix}, \tag{A1}$$

where $\phi'(x)$ and $\phi''(x)$ are first and second derivatives of the first linear eigenfunction of the system that is used to define the waviness, respectively.

and $\beta_r(r=i,\ o)$, $\mathbf{K}_1$, and $\mathbf{K}_2$ given in Eqs. (20) and (21) are defined as follows:

$$\beta_r=\frac{1}{2}\left\{\sum_{n=1}^{N} d_n\left\{\sum_{s=1}^{N} c_{n,ss}^{(1)} W_r\right\}^2\right\}, \tag{A2}$$

$$\mathbf{K}_1=\begin{bmatrix}{}_3W_i^2+3_3W_o^2 & 0 & {}_4W_i^2+3_4W_o^2 & & \ddots & 0 & {}_{N-2}W_i^2+3_{N-2}W_o^2\end{bmatrix}, \tag{A3}$$

$$\mathbf{K}_2=-\begin{bmatrix}{}_3W_o^2+3_3W_i^2 & 0 & {}_4W_o^2+3_4W_i^2 & & \ddots & 0 & {}_{N-2}W_o^2+3_{N-2}W_i^2\end{bmatrix}. \tag{A4}$$

References

[1] S. Iijima, Nature 354 (1991) 56.
[2] D.E.H. Jones, Nature 381 (1996) 384.
[3] R.H. Baughman, A.A. Zakhidov, W.A. de Heer, Science 297 (2002) 787.
[4] C. Li, E.T. Thostenson, T.W. Chou, Compos. Sci. Technol. 68 (2008) 1227.
[5] R.F. Gibson, E.O. Ayorinde, Y.F. Wen, Compos. Sci. Technol. 67 (2007) 1.
[6] G. Hummer, J.C. Rasaiah, J.P. Noworyta, Nature 414 (2001) 188.
[7] J. Liu, A.G. Rinzler, H.J. Dai, J.H. Hafner, R.K. Bradley, P.J. Boul, A. Lu, T. Iverson, K. Shelimov, C.B. Huffman, F. Rodriguez-Macias, Y.S. Shon, T.R. Lee, D.T. Colbert, R.E. Smalley, Science 280 (1998) 1253.
[8] M. Ali-Asgari, H.R. Mirdamadi, M. Ghayour, Physica E 52 (2013) 77.
[9] A. Lohrasebi, H. Raffii-Tabar, J. Mol. Graph. Model. 27 (2008) 116.
[10] H.L. Tang, D.K. Li, S.M. Zhou, Physica E 56 (2014) 306.
[11] Z.B. Shen, L.P. Sheng, X.F. Li, G.J. Tang, Physica E 44 (2012) 1169.
[12] M.B. Panchal, S.H. Upadhyay, Physica E 50 (2013) 73.
[13] Y.M. Fu, J.W. Hong, X.Q. Wang, J. Sound Vib. 296 (2006) 746.
[14] L.Y. Jiang, Y. Huang, H. Jiang, G. Ravichandran, H. Gao, K.C. Hwang, B. Liu, J. Mech. Phys. Solids 54 (2006) 2436.
[15] W.B. Lu, J. Wu, L.Y. Jiang, Y. Huang, K.C. Hwang, B. Liu, Philos. Mag. 87 (2007) 2221.
[16] W.B. Lu, J. Wu, J. Song, K.C. Hwang, L.Y. Jiang, Y. Huang, Comput. Method Appl. Mech. Eng. 197 (2008) 3261.
[17] K.Y. Xu, X.N. Guo, C.Q. Ru, J. Appl. Phys. 99 (2006) 1.
[18] M.H. Mahdavi, L.Y. Jiang, X. Sun, Physica E 43 (2011) 1813.
[19] E. Cigeroglu, H. Samandari, Physica E 46 (2012) 160.
[20] R. Ansari, M. Hemmatnezhad, Nonlinear Dyn. 67 (2012) 373.
[21] R. Bellman, J. Casti, J. Math. Anal. Appl. 34 (1971) 235.
[22] C.W. Bert, M. Malik, J. Press. Vessel Technol. ASME, 19961.
[23] O. Civalek, C. Demir, B. Akgoz, Math. Comput. Appl. 15 (2010) 289.
[24] L. Wang, Q. Ni, Comput. Mater. Sci. 43 (2008) 399.
[25] Y.X. Zhen, B. Fang, Comput. Mater. Sci. 49 (2010) 276.
[26] L.L. Ke, Y. Xiang, J. Yang, S. Kitipornchai, Comput. Mater. Sci. 47 (2009) 409.
[27] M. Janghorban, A. Zare, Physica E 43 (2011) 1602.
[28] R. Ansari, S. Sahmani, Commun. Nonlinear Sci. 17 (2012) 1965.
[29] R. Ansari, M. Hemmatnezhad, Math. Comput. Model. 53 (2011) 927.
[30] A. Farajpour, A.A. Solghar, A. Shahidi, Physica E 47 (2013) 197.
[31] A.H. Nayfeh, B. Balachandran, Applied Nonlinear Dynamics: Analytical, Computational, and Experimental Methods, Wiley, New York, 1995.
[32] M. El-Mously, J. Sound Vib. 261 (2003) 635.
[33] I. Mehdipour, A. Barari, A. Kimiaeifar, G. Domairry, Adv. Eng. Softw. 48 (2012) 1.
[34] Y. Lanir, Y.C.B. Fung, J. Compos. Mater. 6 (1972) 387.
[35] P.M. Jelf, N.A. Fleck, J. Compos. Mater. 26 (1992) 2706.
[36] J. Yoon, C.Q. Ru, A. Mioduchowski, J. Appl. Mech.-Trans. ASME 72 (2005) 10.
[37] A.A. Abrikosov, L.P. Gorkov, I.E. Dzyaloshinskii, Sov. Phys. JETP-USSR 9 (1959) 636.
[38] W. Burghard, Kriminalistik 54 (2000) 628.
[39] P. Soltani, P. Bahar, A. Farshidianfar, Proc. Inst. Mech. Eng. C-J. Mech. 225 (2011) 1730.
[40] F.N. Mayoof, M.A. Hawwa, Chaos Soliton Fractals 42 (2009) 1860.
[41] C. Shu, B.E. Richards, Int. J. Numer. Methods Fluids 15 (1992) 791.
[42] C.W. Bert, M. Malik, Appl. Mech. Rev. 49 (1996) 1–28.
[43] M. Danesh, A. Farajpour, M. Mohammadi, Mech. Res. Commun. 39 (2012) 23.
[44] M. Abramowitz, I.A. Stegun, Handbook of Mathematical Functions with Formulas, Graphs, and Mathematical Tables, U.S. Govt. Print. Off., Washington, 1964.
[45] H. Samandari, E. Cigeroglu, Nonlinear free vibration of curved double walled carbon nanotubes using differential quadrature method, in: G. Kerschen, D. Adams, A. Carrella (Eds.), Topics in Nonlinear Dynamics, 1, Springer, New York, 2013, pp. 269–279.